JOURNAL OF COMPUTATIONAL PHYSICS 46, 342–368 (1982)

Adaptive Zoning for Singular Problems in Two Dimensions*

J. U. BRACKBILL AND J. S. SALTZMAN

Applied Theoretical Physics Division, Los Alamos National Laboratory, Los Alamos, New Mexico 87545

Received February 26, 1981; revised September, 28, 1981

Winslow's method for the automatic generation of computation meshes is extended to adaptively vary the zone sizes and orthogonality of grid lines in the resulting mesh. Through simple analysis and numerical examples, the adaptive mesh is shown to give significant increases in accuracy in the computation of singular problems.

I. INTRODUCTION

Winslow's method [1] for the automatic generation of computation meshes is extended to give discretionary control of the variation of zone sizes and orthogonality of grid lines in the resulting mesh. The additional control is used to adapt the mesh to the problem to increase the accuracy of the result.

Winslow formulates the zoning problem "as a potential problem with the mesh lines playing the role of equipotentials" [1]. The formulation requires the solution of a nonlinear, Poisson-like equation to generate a mapping from a regular domain in a parameter space to an irregularly shaped domain in physical space. By connecting points in the physical space corresponding to discrete points in the parameter space, the physical domain can be covered with a computation mesh suitable for the solution of finite difference equations.

Winslow's method is widely used, especially for exterior flow problems. His method has received attention from Godunov and Prokopov [2], and from Thompson *et al.* [3] among others. Godunov devised an algorithm for generating meshes for initial boundary value problems, in which changes in the boundary data are reflected in changes in the mesh. Thompson developed a method for generating body-fitted coordinates in multiply connected domains. The popularity of these methods arises primarily from their usefulness in giving accurate, numerical representation of the boundary geometry. For example, when calculating flow past an airfoil, the geometry of the boundary is important and its accurate representation is essential to the

* This work was performed under the auspices of the United States Department of Energy.

0021-9991/82/060342-27$02.00/0

accuracy of the overall calculation. Thompson's codes applying Winslow's method make shaping the boundary convenient.

If, however, resolution within the boundary layer in the airfoil problem were also important, or, as in the case of many flow problems, an embedded region with strong gradients were to develop, control of the spacing of the mesh far from the boundaries becomes as desirable as accurate representation of the geometry of the boundary. In reaction diffusion processes, in resistive magnetohydrodynamic flow, and in shocked flows, singular regions may develop far from the boundaries. For these, new methods must be developed which somehow adapt to the data in the interior as well as conform to the shape of the boundaries.

Constructing adaptive mesh generators, those which alter themselves in response to changes in the data, is an area of current interest [4–10, 18]. In many recent studies, adaptiveness results from inhomogeneous terms added to the potential equations. For example, terms may be added to control the spacing of zones to increase resolution in regions of strong gradients [5, 18]. In others, zones are added to regions of the mesh to distribute the error equally [10].

These studies have shown the value of adaptive zoning, and applications have shown the usefulness of mesh generators of Winslow's type [11, 12]. Toward the goal of devising a mesh generator appropriate for arbitrarily shaped domains which both maintains logical connectivity and adapts to the data, we have combined certain ideas of Winslow [1], Browne [13] (who used a variational formulation of Winslow's method similar to Belinskii *et al.* [21]), and Barfield [14] in a variational formulation similar to one developed independently by Yanenko *et al.* [19].

The unifying idea is that a mesh generator can be formulated to optimize several measurable properties of the computation mesh simultaneously. Optimizing smoothness [1], orthogonality [14], and the variation in cell volumes together gives the interior control of the mesh needed for adaptive zoning. The discretion the user retains in determining the relative importance given to the optimization of each of these properties, or to other properties controlled in the same way, allows him to fit the adaptive mesh to the problem.

It is the purpose of this paper to expand the description of the adaptive mesh generator contained in several earlier papers [20], and to present a number of numerical examples illustrating its application to singular problems.

II. Formulation of the Mesh Generator

For the solution of finite difference equations on a computation mesh, the data is typically stored in ordered arrays of numbers, $\phi(i,j)$ in which the indices $i = 1,..., M$; $j = 1,..., N$, give not only the location of the data in computer memory, but also the physical relationship between the data at one vertex $\mathbf{x}(i,j)$ and another, $\mathbf{x}(i',j')$. For example, in a mesh of quadrilateral cells, the neighbors of $\mathbf{x}(i,j)$ are $\mathbf{x}(i+1,j)$, $\mathbf{x}(i,j+1)$, $\mathbf{x}(i-1,j)$, and $\mathbf{x}(i,j-1)$.

In formulating the mesh generator problem mathematically, it is useful to view the

mesh, whose vertices are $\mathbf{x}(i,j)$, as the image of a mapping $\mathbf{x}(\xi, \eta)$ in which only the points corresponding to integer values of the natural coordinates ξ and η are realized. (Conversely, the image of a computation mesh of quadrilateral cells is a uniform, rectilinear mesh in (ξ, η) space with spacing $\Delta\xi = \Delta\eta = 1$.) A mesh generator determines the mapping $\mathbf{x}(\xi, \eta)$.

A useful observation is that the differential properties of the mapping determine the properties of the computation mesh. For example, $[(\partial x/\partial\xi)^2 + (\partial y/\partial\xi)^2]^{1/2}$ along a level curve of η is related to mesh spacing between vertices with same index j. Similarly, the volume of computational cells is related to the Jacobian J of the mapping

$$J = \frac{\partial x}{\partial \xi}\frac{\partial y}{\partial \eta} - \frac{\partial x}{\partial \eta}\frac{\partial y}{\partial \xi}, \tag{1}$$

and the orthogonality of the mesh is related to the scalar, $\nabla\xi \cdot \nabla\eta$, which is zero when conjugate lines of the mesh are orthogonal.

Integrals over the computation mesh can be written which measure these properties of the mapping. The global smoothness of the mapping (the variation in mesh spacing along level curves of ξ and η) is measured by the integral

$$I_s = \int_D [(\nabla\xi)^2 + (\nabla\eta)^2]\, dV. \tag{2}$$

The orthogonality of the mapping is measured by

$$I_o = \int_D (\nabla\xi \cdot \nabla\eta)^2\, dV, \tag{3a}$$

or the volume weighted measure

$$I_o' = \int_D (\nabla\xi \cdot \nabla\eta)^2 J^3\, dV$$

and the weighted volume variation is measured by

$$I_v = \int_D wJ\, dV, \tag{4}$$

where $w = w(x, y)$ is a given function.

Of course, if a property can be measured, it can be controlled. The smoothest mapping can be obtained by minimizing I_s, the most orthogonal mapping by minimizing I_o', and the mapping withspecified variation of J by minimizing I_v. It is not possible, however, to minimize I_o' or I_v separately, because the solutions to the corresponding minimization problems do not have unique solutions.

For example, consider a weighted volume variation problem with $w \equiv 1$ and a

solution $x_0(\xi, \eta)$, $y_0(\xi, \eta)$. Then $wJ = J_0 = \text{const}$. From this solution, a one-parameter (t) family of solutions can be constructed such that

$$x(\xi, \eta, t=0) = x_0(\xi, \eta),$$
$$y(\xi, \eta, t=0) = y_0(\xi, \eta),$$

where velocities and a Jacobian are defined by

$$u(\xi, \eta, t) \equiv \frac{\partial x(\xi, \eta, t)}{\partial t},$$
$$v(\xi, \eta, t) \equiv \frac{\partial y(\xi, \eta, t)}{\partial t},$$

and

$$J(\xi, \eta, t) \equiv x_\xi(\xi, \eta, t)\, y_\eta(\xi, \eta, t) - x_\eta(\xi, \eta, t)\, y_\xi(\xi, \eta, t).$$

Using Eqs. (5a)–(5d) below results in

$$\frac{1}{J}\frac{\partial J}{\partial t} = \frac{\partial u}{\partial x} + \frac{\partial v}{\partial y}.$$

Clearly, $J(t) = J_0$ if the velocity field is incompressible,

$$\frac{\partial u}{\partial x} + \frac{\partial v}{\partial y} = 0.$$

Since any potential flow is incompressible, a one-parameter family of solutions to the weighted volume variation problem with $J(t) = J_0$ can be constructed. Where $(u, v) = \nabla\psi$, and $\hat{n}$ is the unit normal to the boundary, ψ is given by the solution of the equation

$$\nabla^2\psi = 0,$$

with $\hat{n} \cdot \nabla\psi = 0$ on the boundary. (Similarly, orthogonal meshes can be folded to generate new orthogonal meshes.)

Thus, to formulate minimization problems with unique solutions, the minimization of I_0' or I_v is combined with I_s (which has a unique solution [3]) as in the penalty method [15]. That is, the integral I is minimized, where

$$I = I_s + \lambda_v I_v + \lambda_0' I_0',$$

with $\lambda_v \geqslant 0$, $\lambda_0' \geqslant 0$. In Section IV, it is shown by calculation that numerical solutions which minimize I are obtained for finite values of λ_v and λ_0'.

III. Solution of the Variational Problem in Two Dimensions

To derive the Euler equations for the variational problem formulated in the preceeding section, it is first convenient to interchange dependent and independent variables using the relations

$$\xi_x = + y_\eta / J, \tag{5a}$$

$$\xi_y = - x_\eta / J, \tag{5b}$$

$$\eta_x = - y_\xi / J, \tag{5c}$$

and

$$\eta_y = + x_\xi / J. \tag{5d}$$

After interchanging variables, the smoothness measure can be written

$$I_s = \int_1^M \int_1^N d\xi \, d\eta \, \frac{x_\xi^2 + x_\eta^2 + y_\xi^2 + y_\eta^2}{J}, \tag{6}$$

for which the corresponding Euler equations are

$$\left(\frac{\partial}{\partial x} - \frac{\partial}{\partial \xi}\frac{\partial}{\partial x_\xi} - \frac{\partial}{\partial \eta}\frac{\partial}{\partial x_\eta}\right)\left(\frac{x_\xi^2 + x_\eta^2 + y_\xi^2 + y_\eta^2}{J}\right) = 0, \tag{7a}$$

$$\left(\frac{\partial}{\partial y} - \frac{\partial}{\partial \xi}\frac{\partial}{y_\xi} - \frac{\partial}{\partial \eta}\frac{\partial}{\partial y_\eta}\right)\left(\frac{x_\xi^2 + x_\eta^2 + y_\xi^2 + y_\eta^2}{J}\right) = 0. \tag{7b}$$

Performing the indicated differentiation and collecting coefficients of the highest derivatives yields the equations

$$B(\alpha x_{\xi\xi} - 2\beta x_{\xi\eta} + \gamma x_{\eta\eta}) - A(\alpha y_{\xi\xi} - 2\beta y_{\xi\eta} + \gamma y_{\eta\eta}) = 0, \tag{8a}$$

$$-A(\alpha x_{\xi\xi} - 2\beta x_{\xi\eta} + \gamma x_{\eta\eta}) + C(\alpha y_{\xi\xi} - 2\beta y_{\xi\eta} + \gamma y_{\eta\eta}) = 0, \tag{8b}$$

where

$$A = x_\xi y_\xi + x_\eta y_\eta, \qquad B = y_\xi^2 + y_\eta^2, \qquad C = x_\xi^2 + x_\eta^2, \tag{9}$$

and

$$\alpha = (x_\eta^2 + y_\eta^2)/J^3, \qquad \beta = (x_\xi x_\eta + y_\xi y_\eta)/J^3, \qquad \gamma = (x_\xi^2 + y_\xi^2)/J^3. \tag{10}$$

Of course, when $A^2 - BC \neq 0$, the Euler equations can be factored and the equations written in the form given by Winslow [1],

$$\alpha x_{\xi\xi} - 2\beta x_{\xi\eta} + \gamma x_{\eta\eta} = 0, \tag{11a}$$

$$\alpha y_{\xi\xi} - 2\beta y_{\xi\eta} + \gamma y_{\eta\eta} = 0. \tag{11b}$$

Factorization, however, is not possible in the composite Euler equations and so it will be useful later to have the equations in standard form

$$b_{s1}x_{\xi\xi} + b_{s2}x_{\xi\eta} + b_{s3}x_{\eta\eta} + a_{s1}y_{\xi\xi} + a_{s2}y_{\xi\eta} + a_{s3}y_{\eta\eta} = 0 \tag{12a}$$

and

$$a_{s1}x_{\xi\xi} + a_{s2}x_{\xi\eta} + a_{s3}x_{\eta\eta} + c_{s1}y_{\xi\xi} + c_{s2}y_{\xi\eta} + c_{s3}y_{\eta\eta} = 0, \tag{12b}$$

where

$$\begin{aligned} a_{s1} &= -A\alpha, & b_{s1} &= B\alpha, & c_{s1} &= C\alpha, \\ a_{s2} &= 2A\beta, & b_{s2} &= -2B\beta, & c_{s2} &= -2C\beta, \\ a_{s3} &= -A\gamma, & b_{s3} &= B\gamma, & c_{s3} &= C\gamma. \end{aligned} \tag{13}$$

The measure of volume variation, after interchanging dependent and independent variables, can be written

$$I_v = \int_1^M \int_1^N d\xi\, d\eta\, wJ^2, \tag{14}$$

for which the Euler equations are

$$\frac{\partial w}{\partial x} J^2 - 2[J(w_\xi y_\eta - w_\eta y_\xi) + w(J_\xi y_\eta - J_\eta y_\xi)] = 0 \tag{15a}$$

and

$$\frac{\partial w}{\partial y} J^2 - 2[J(x_\xi w_\eta - x_\eta w_\xi) + w(x_\xi J_\eta - x_\eta J_\xi)] = 0. \tag{15b}$$

Collecting coefficients of the highest derivatives yields the equations

$$2w(b_{v1}x_{\xi\xi} + b_{v2}x_{\xi\eta} + b_{v3}x_{\eta\eta} + a_{v1}y_{\xi\xi} + a_{v2}y_{\xi\eta} + a_{v3}y_{\eta\eta}) = -J^2 \frac{\partial w}{\partial x} \tag{16a}$$

and

$$2w(a_{v1}x_{\xi\xi} + a_{v2}x_{\xi\eta} + a_{v3}x_{\eta\eta} + c_{v1}y_{\xi\xi} + c_{v2}y_{\xi\eta} + c_{v3}y_{\eta\eta}) = -J^2 \frac{\partial w}{\partial y}, \tag{16b}$$

where the coefficients are given by

$$\begin{aligned} a_{v1} &= -x_\eta y_\eta, & b_{v1} &= y_\eta^2, & c_{v1} &= x_\eta^2, \\ a_{v2} &= x_\xi y_\eta + x_\eta y_\xi, & b_{v2} &= -2y_\xi y_\eta, & c_{v2} &= -2x_\xi x_\eta, \\ a_{v2} &= -x_\xi y_\xi, & b_{v3} &= y_\xi^2, & c_{v3} &= x_\xi^2. \end{aligned} \tag{17}$$

Similarly, the orthogonality measure I_0' can be written

$$I_0' = \int_1^M \int_1^N d\xi\, d\eta (x_\xi x_\eta + y_\xi y_\eta)^2, \tag{18}$$

for which the Euler equations are

$$b_{01} x_{\xi\xi} + b_{02} x_{\xi\eta} + b_{03} x_{\eta\eta} + a_{01} y_{\xi\xi} + a_{02} y_{\xi\eta} + a_{03} y_{\eta\eta} = 0 \tag{19a}$$

and

$$a_{01} x_{\xi\xi} + a_{02} x_{\xi\eta} + a_{03} x_{\eta\eta} + c_{01} y_{\xi\xi} + c_{02} y_{\xi\eta} + c_{03} y_{\eta\eta} = 0, \tag{19b}$$

with coefficients

$$\begin{aligned} a_{01} &= x_\eta y_\eta, & b_{01} &= x_\eta^2, & c_{01} &= y_\eta^2, \\ a_{02} &= x_\xi y_\eta + x_\eta y_\xi, & b_{02} &= 2(2x_\xi x_\eta + y_\xi y_\eta), & c_{02} &= 2(x_\xi x_\eta + 2y_\xi y_\eta), \\ a_{03} &= x_\xi y_\xi, & b_{03} &= x_\xi^2, & c_{03} &= y_\xi^2. \end{aligned} \tag{20}$$

In general, the Euler equations are to be added together with coefficients given by

$$\begin{aligned} a &= a_s + \lambda_v a_v + \lambda_0' a_0, \\ b &= b_s + \lambda_v b_v + \lambda_0' b_0, \\ c &= c_s + \lambda_v c_v + \lambda_0' c_0, \end{aligned} \tag{21}$$

where λ_v and λ_0' are positive constants.

IV. Numerical Solution

To generate a mapping, finite difference approximations to the Euler equations are solved by iteration. Since (ξ, η) are continuous variables which take on integer values at the nodes of the computation mesh, they form a uniformly spaced, rectilinear grid in parameter space. The derivatives with respect to the independent variables are easily computed on this grid. Where each node of the mesh is labelled by the value of (ξ, η) at the node, namely (i,j), the value of the derivatives at the nodes are approximated by the difference equations

$$\begin{aligned} x_\xi &\simeq \tfrac{1}{2}(x_{i+1,j} - x_{i-1,j}), \\ x_\eta &\simeq \tfrac{1}{2}(x_{i,j+1} - x_{i,j-1}), \end{aligned} \tag{22}$$

and the second derivatives by

$$x_{\xi\xi} = x_{i+1,j} - 2x_{i,j} + x_{i-1,j},$$
$$x_{\xi\eta} = \tfrac{1}{4}(x_{i+1,j+1} + x_{i-1,j-1} - x_{i+1,j-1} - x_{i-1,j+1}) \tag{23}$$

$$x_{\eta\eta} = x_{i,j+1} - 2x_{i,j} + x_{i,j-1}, \tag{24}$$

and similarly for y. Algebraic equations at each node result from the substitution of the differences for derivatives. The system of equations is solved by a Jacobi iteration in which the values of $x_{i,j}$ and $y_{i,j}$ are treated as parameters. R_x and R_y are the residual errors defined by

$$R_x = (R_s)_x + \lambda_v(R_v)_x + \lambda_o(R_o)_x,$$
$$R_y = (R_s)_y + \lambda_v(R_v)_y + \lambda_o(R_o)_y. \tag{25}$$

where R_s, R_v, and R_o are residuals of Eqs. (12), (16), and (19), respectively. Letting (l) be the iteration number, the values of $x_{i,j}^{(l+1)}$ and $y_{i,j}^{(l+1)}$ are calculated from the equations

$$0 = R_x^{(l)} + \frac{\partial R_x^{(l)}}{\partial x_{ij}}(x_{ij}^{(l+1)} - x_{ij}^{(l)}) + \frac{\partial R_x^{(l)}}{\partial y_{ij}}(y_{ij}^{(l+1)} - y_{ij}^{(l)}) \tag{26a}$$

and

$$0 = R_y^{(l)} + \frac{\partial R_y^{(l)}}{\partial x_{ij}}(x_{ij}^{(l+1)} - x_{ij}^{(l)}) + \frac{\partial R_y^{(l)}}{\partial y_{ij}}(y_{ij}^{(l+1)} - y_{ij}^{(l)}), \tag{26b}$$

where

$$\frac{\partial R_x^{(l)}}{\partial x_{ij}} = -2(b_1 + b_3),$$
$$\frac{\partial R_x^{(l)}}{\partial y_{ij}} = -2(a_1 + a_3) = \frac{\partial R_y^{(l)}}{\partial x_{ij}}, \tag{27}$$
$$\frac{\partial R_y^{(l)}}{\partial y_{ij}} = -2(c_1 + c_3).$$

The iteration continues until $R_x^{(l)}$ and $R_y^{(l)}$ are everywhere less than the maximum allowed error.

V. Numerical Examples

The effect of minimizing $I_s + \lambda_v I_v$ rather than I_s alone (Winslow's mesh generator) is illustrated by a simple numerical example. With w given by

$$w = [\sin(2\pi x/X)\sin(2\pi y/Y) + 1 + (1/\sigma)], \tag{28a}$$

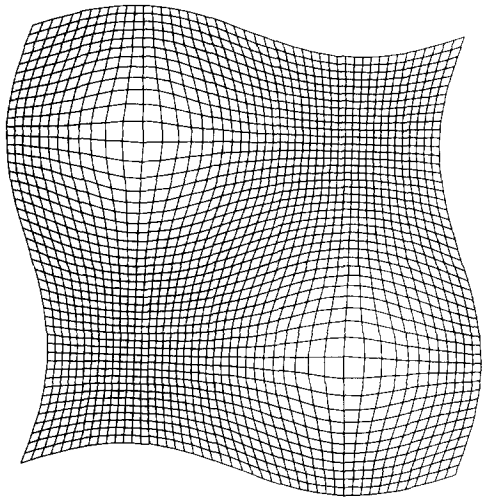

FIG. 1. With $r = 100$, $\lambda_v = 4$, and periodic boundary conditions, minimizing $I_s + \lambda I_v$ gives the mesh shown.

where X and Y are the periodic lengths in x and y, and $2\sigma + 1$ ($\geqslant 1$) is the ratio of the maximum to minimum value of the weight function and w positive everywhere. Meshes are generated with periodic boundary conditions for a sequence of λ_v, $0 \leqslant \lambda_v \leqslant 16$. With $X = Y = 1$, $M = N = 50$, and $\lambda_v = 0$, Winslow's generator gives a uniform, rectilinear mesh. With $\sigma = 100$ and $\lambda_v = 4$, Winslow's generator plus the volume modifier gives the mesh shown in Fig. 1. In the modified mesh, where w is large $[(x, y) = (\frac{1}{4}, \frac{1}{4})]$, the cells are small, and where w is small $[(x, y) = \frac{3}{4}, \frac{1}{4})]$, the cells are large.

The results with several values of λ_v, $0 \leqslant \lambda_v \leqslant 16$, are summarized in Fig. 2, where I_s, I_v, and the maximum and minimum cell volumes are plotted for a mesh with

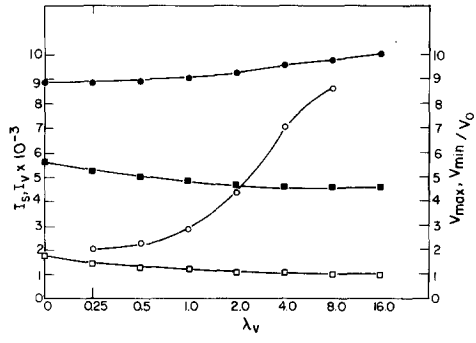

FIG. 2. The values of I_s, I_v, and the maximum and minimum cell volumes are plotted for various values of I_v. Note that V_{min} decreases less than V_{max} increases from its value for $\lambda_v = 0$. ●, I_s; ■, I_v; ○, V_{max}; □, V_{min}.

TABLE I

$I/J = 25/25$, $\sigma = 100$

λ_v	V_{max}	V_{min}	V_{max}/V_{min}
0.00	1.74-3	1.74-3	1.00
0.25	2.01-3	1.43-3	1.41
0.5	2.28-3	1.30-3	1.75
1.0	2.89-3	1.17-3	2.47
2.0	4.36-3	1.06-3	4.11
4.0	7.06-3	9.85-4	7.17
8.0	8.60-3	9.40-4	9.15
16.0	—	9.04-4	—

$\sigma = 100$, and $M = N = 25$. As λ_v increases, I_v, which measures the variance in wJ^2 over the mesh, decreases as the solution $wJ^2 = \text{const}$ is approached. Correspondingly, the maximum cell volume increases and the minimum decreases, although the asymptotic value of the minimum seems to be reached for smaller values of λ_v, and the ratio V_{max}/V_{min} approaches the prescribed value $\sqrt{2\sigma + 1}$ as shown in Table I. However, I_s, which measures the smoothness of the mapping, increases with increasing λ_v. As expected, volume variation is obtained at the expense of smoothness.

Similar control of the volume variation is obtained nearly independently of the direction of variation of w with respect to the principal directions. When w is given by

$$w = \sin(2\pi x/X) + 1 + (1/\sigma), \tag{28b}$$

with $\lambda_v = 2$ and $\sigma = 100$ the mesh shown in Fig. 3 results. The cell volumes vary only in the x direction, with a maximum volume equal to 2.94 (relative to the unweighted cell volume) and a minimum equal to 0.59 for a ratio of maximum to minimum equal to 4.98. (This is one third the prescribed ratio $\sqrt{2\sigma + 1}$ between maximum and minimum value.) When w is given by

$$w = \sin[4\pi(x + y)/(X + Y)] + 1 + (1/\sigma), \tag{28c}$$

so that w varies along the diagonal of the mesh, the mesh shown in Fig. 4 results with $\lambda_v = 2$ and $\sigma = 100$. The cell volumes vary along the diagonal of the mesh, with a maximum volume equal to 2.75 and a minimum equal to 0.62 for a ratio of maximum to minimum equal to 4.44. The 10% difference between this and the ratio above supports the conclusion that the ability to control volume is not strongly dependent on the direction of the gradient in w relative to the principal directions. We also note that, by direct measurement, the ratio of the minimum distance between vertices along the gradient of w in Fig. 3 to the corresponding distance (along the diagonal) in Fig. 4 is $1/\sqrt{2}$, exactly the ratio one would obtain on a rectilinear mesh between the side and the diagonal.

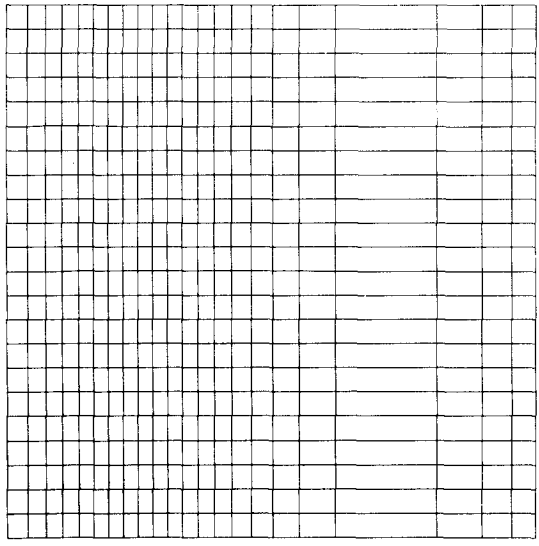

FIGURE 3

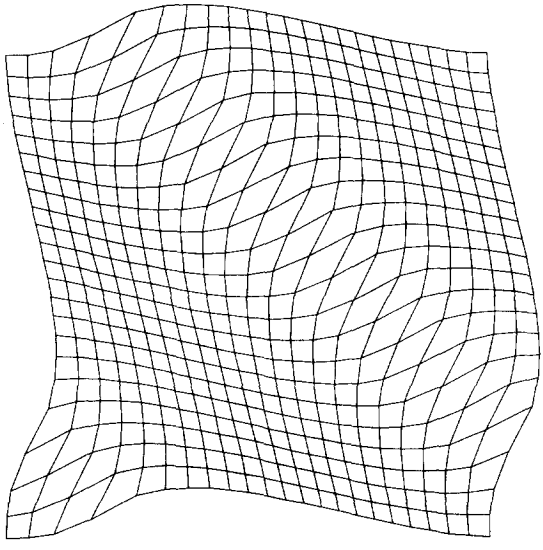

FIGURE 4

FIGS. 3, 4. The responsiveness of the volume control is nearly inependent of the direction of the gradient of the weight function relative to the principal directions. The volume variation in Fig. 3, with $w = f(x)$, is the same as in Fig. 4, with $w = f(x + y)$.

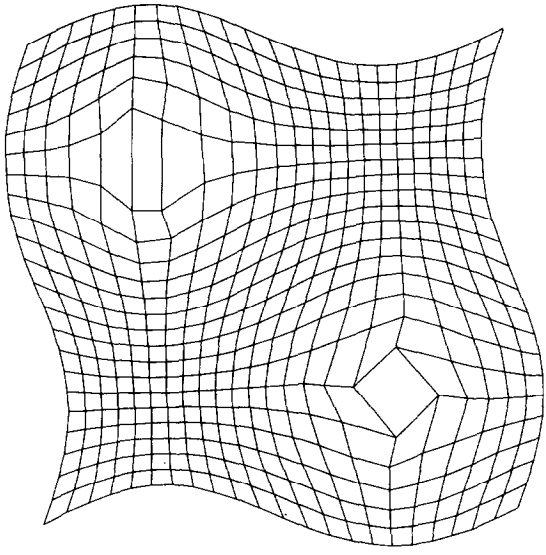

FIGURE 5

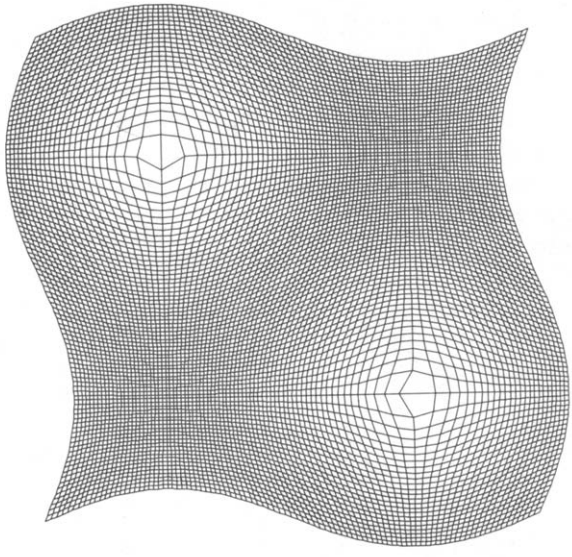

FIGURE 6

FIGS. 5, 6. The maximum value of λ_v is influenced by the number of cells in the mesh. With $\lambda_v = 16$, a solution is obtained with the 99×99 mesh in Fig. 6, but not with the 25×25 mesh in Fig. 5.

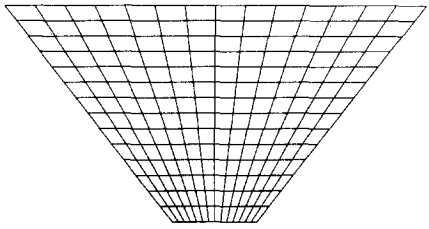

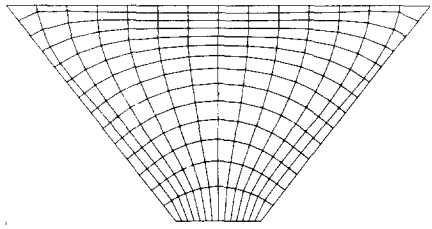

FIGS. 7, 8. When $I_s + \lambda_0 I_0'$ is minimized, the mesh is made more orthogonal. In Fig. 7 (left), $\lambda_0 = 0$; in Fig. 8 (right), $\lambda_0 = 10^3$.

Finally, to determine how closely the computed ratio of cell volumes can be made to approach the prescribed value, λ_v is made as large as possible. Earlier it was shown that the solution to the minimization problem with $\lambda_v \to \infty$ is not unique. However, only numerical solutions can show how large λ_v can be. With w given by Eq. (28a), $M = N = 25$, $\lambda_v = 16$, the mesh shown in Fig. 5 is obtained. The largest cells in the mesh are distorted. Not only that, but the iteration does not converge. The maximum volume fluctuates from cycle to cycle even though I_v, I_s and the minimum volume are nearly constant. With $M = N = 99$ and $\lambda_v = 16$, however, the solution shown in Fig. 6 is obtained. This time, the iteration converges. Since the difference between the two cases is the number of zones, the largest value of λ_v for which solutions can be obtained successfully is obviously influenced by numerical accuracy, but seems to be $\lambda_v \leqslant O(10)$.

The effect of minimizing $I_s + \lambda_0' I_0'$ (Eqs. (16) and (18)) rather than I_s alone is illustrated by the solutions depicted in Figs. 7–9. For $\lambda_0' = 0$, a mesh has been generated with Winslow's generator (Eq. (6)) with Dirichlet boundary conditions and is shown in Fig. 7. Because the boundaries are skew, the intersections of mesh lines are also skew. Increasing λ_0 to 1000 results in the mesh shown in Fig. 8. The intersections of mesh lines appear to be more nearly orthogonal. That the mesh is increasingly orthogonal as λ_0 is increased is demonstrated by the results shown in Fig. 9, where the variation of I_0' with λ_0' is plotted. As λ_0' increases from 0 to 10,000,

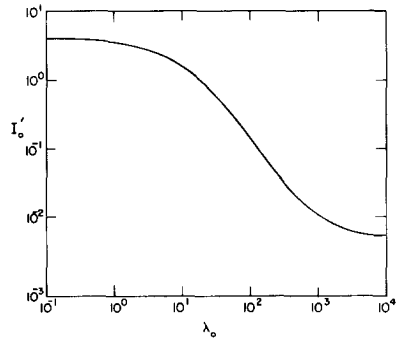

FIG. 9. Corresponding to the meshes shown in Figs. 7 and 8, I_0' decreases as λ_0 increases.

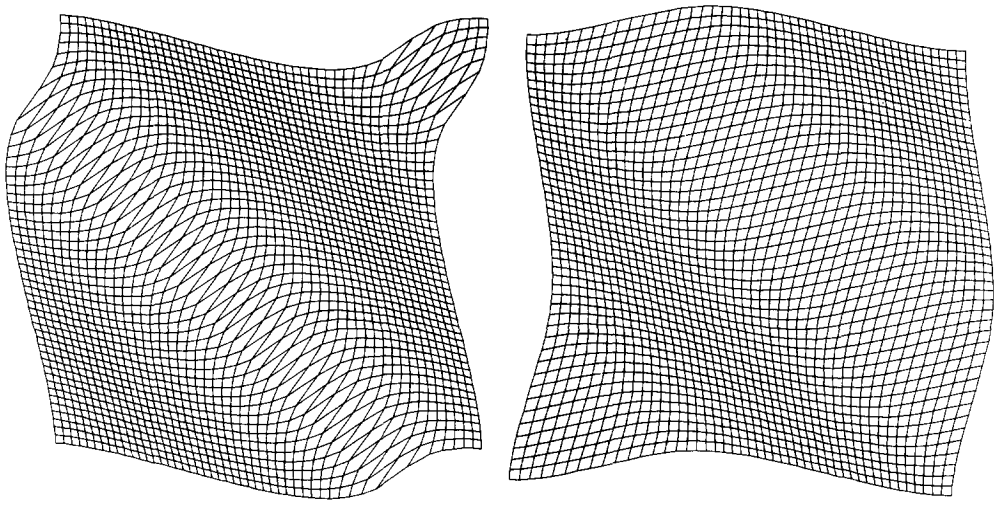

FIGS. 10, 11. Increasing λ_0 decreases the skewness of the mesh as shown by comparing Fig. 10 (left) with $\lambda_0 = 0$ with Fig. 11 (right) with $\lambda_0 = 1$.

I_0 decreases from 4 to 0.006. Thus, the minimization appears to have the desired effect.

When $I_s + \lambda_v I_v + \lambda_0' I_0'$ is minimized, increasing λ_0' from zero decreases the skewness of the mesh. With w given by Eq. (28c), $M = N = 50$, $\lambda_v = 4$, and $\lambda_0' = 0$, the mesh shown in Fig. 10 is obtained. The largest zones are quite skew. When $\lambda_0 = 1$, the mesh shown in Fig. 11 results. The skewness is considerably reduced. The maximum zone size is reduced, however, so that the decrease in skewness is accompanied by a decrease in volume control.

VI. The Adaptive Mesh

The mesh generator described above will now be made part of an algorithm to adapt a computation mesh dynamically to data generated by the solution of finite difference equations. Adapting the mesh will be shown to reduce numerical error when the resolution of gradients is improved.

In developing the adaptive algorithm, it is useful to consider Burger's equation in one dimension,

$$\frac{\partial u}{\partial t} + (u + V)\frac{\partial u}{\partial x} - \kappa \frac{\partial^2 u}{\partial x^2} = 0, \tag{29}$$

where κ and $V > 0$ are constant. A steady solution to Burger's equation is given by

$$u = (u_0/2)(g^- - g^+), \tag{30}$$

where g^- and g^+ are written

$$g^- = \left(1 + \exp \frac{-u_0(x - Vt)}{\kappa}\right)^{-1} \tag{31a}$$

and

$$g^+ = \left(1 + \exp \frac{u_0(x - Vt)}{\kappa}\right)^{-1}. \tag{31b}$$

This solution corresponds to a progressing wave propagating in the positive x direction with speed V.

The solution above is typical for a singular perturbation problem for, as $\kappa \to 0$, it is nearly constant everywhere except in the small interval $(Vt - \kappa/u_0) < x < (Vt + \kappa/u_0)$. There, the derivative of u, written

$$\frac{\partial u}{\partial x} = \frac{u_0^2}{\kappa} g^+ g^-, \tag{32}$$

$$\frac{\partial^n u}{\partial x^n} = O(\kappa^{-n}). \tag{33}$$

There are obvious difficulties in treating problems of this type numerically, for the truncation error becomes very large as $\kappa \to 0$. Consider a typical finite-difference approximation to the derivative

$$\left\langle \frac{\partial u}{\partial x} \right\rangle = \frac{u_{i+1} - u_{i-1}}{x_{i+1} - x_{i-1}}. \tag{34}$$

Where the mesh interval is written

$$\nabla = \tfrac{1}{2}(x_{i+1} - x_{i-1}), \tag{35}$$

and a grid Reynolds number is defined by

$$R_e \equiv u_0 \nabla / \kappa, \tag{36}$$

by substitution of the solution, Eq. (30) into Eq. (34), we find

$$\lim_{R_e \to \infty} \left\langle \frac{\partial u}{\partial x} \right\rangle = \frac{u_0}{2\nabla}. \tag{37}$$

However, the correct value from Eq. (33) for $\partial u/\partial x$ scales as R_e. Thus, the relative error ε in the approximation of the derivative becomes large,

$$\lim_{R_e \to \infty} (\varepsilon) = \lim_{R_e \to \infty} \left(\left\langle \frac{\partial u}{\partial x} \right\rangle - \frac{\partial u}{\partial x} \right) \Big/ \left(\frac{\partial u}{\partial x} \right) = -1. \tag{38}$$

The cause is obvious. The narrow region where $(\partial u/\partial x)$ is large is not resolved by a uniform mesh when $R_e \gg 1$.

In contrast, the error on an adaptive mesh generated by minimizing the weighted volume variation with w chosen to resolve gradients of u,

$$w = \left[\frac{1}{(u+u_0)}\frac{\partial u}{\partial x}\right]^2 \tag{39}$$

scales differently. In one dimension, since $J = x_\xi$ minimizing the integral I_v of Eq. (14) minimizes x_ξ where $\partial u/\partial x$ is large, the resolution of the singular region is improved.

The effect of varying x_ξ on the truncation error is estimated by repeating the analysis above. The mesh spacing is given by

$$\left(\frac{\partial u}{\partial x}\right)^2 x_\xi^2 = c(u+u_0)^2. \tag{40}$$

The constant of integration c, is determined by the number N of mesh points in the computational domain, $-X \leqslant x \leqslant X$, which is given by

$$N = \int_{-X}^{X} \xi_x' \, dx' = \frac{2u_0}{\kappa\sqrt{c}} \int_{-X}^{X} \left[\frac{g^+ g^-}{(g^- - g^+) + 2}\right] dx. \tag{41}$$

The integral is everywhere positive, and for $u_0 X \gg \kappa$ is given by

$$N \cong 1/\sqrt{c}. \tag{42}$$

At the symmetry point where $u = 0$, x_ξ is given by

$$x_\xi = 4\kappa/u_0 N. \tag{43}$$

For a nonuniform mesh, the truncation error (which is estimated by substituting the correct solution into the difference equation and expanding about $u(x_i)$) can be written

$$\begin{aligned}\left(\frac{\partial u}{\partial x}\right)\varepsilon &= \left(\frac{u_{i+1}-u_{i-1}}{x_{i+1}-x_{i-1}} - \frac{\partial u}{\partial x}\right) \\ &= \left\{\frac{1}{2}\frac{\partial^2 u}{\partial x^2}\frac{(\nabla+\delta)^2-(\nabla-\delta)^2}{2\nabla} + \frac{1}{6}\frac{\partial^3 u}{\partial x^3}\frac{(\nabla+\delta)^3+(\nabla-\delta)^3}{2\nabla}\right. \\ &\quad \left. + \cdots + \frac{1}{n!}\frac{\partial^n u}{\partial x^n}\frac{(\nabla+\delta)^n - [-(\nabla-\delta)]^n}{2\nabla} + \cdots\right\},\end{aligned} \tag{44}$$

where

$$\delta = \tfrac{1}{2}[(x_{i+1}-x_i) - (x_i - x_{i-1})].$$

The derivatives can be evaluated from the recursion relation which the steady solution to Burger's equation in the wave frame satisfies

$$\frac{\partial^2 u}{\partial x^2} = \frac{u}{\kappa}\frac{\partial u}{\partial x}.$$

By differentiation, one finds that

$$\begin{aligned} \frac{\partial^n x}{\partial \xi^n} &= O(\kappa^n), \qquad n \text{ odd}, \\ \frac{\partial^n x}{\partial \xi^n} &= 0, \end{aligned} \tag{45}$$

Thus it will not alter the scaling of the truncation error if the substitution

$$x_\xi^{n-1} = \frac{(\nabla + \delta)^n - [-(\nabla - \delta)^n]}{2\nabla} \tag{46}$$

is made. With this approximation, the truncation error at the point of symmetry is given by

$$\varepsilon = \frac{1}{4}\sum_m \frac{1}{(2m+1)!}\left(\frac{1}{N}\right)^{2m}. \tag{47}$$

In contrast to the relative error for the nonadaptive grid, Eq. (39), the relative error for the adaptive grid does not increase as $\kappa \to 0$.

The conclusion one can draw from this simple example is that, by the proper choice of volume weight function, the effect of the singular nature of the solution on numerical truncation error can be mitigated. That this is true in two dimensions as well will now be shown.

In extending the adaptive mesh to two dimensions, a heuristic approach is taken. It is first shown that the two-dimensional adaptive mesh reduces to the apropriate one-dimensional limit for a one-dimensional problem. Next, the results of a computation in two dimensions are presented which illustrate the increase in accuracy obtained with an adaptive mesh.

First, consider a problem in two dimensions where w is given by

$$w = (\phi^{-1}\nabla\phi)^2, \tag{48}$$

where $\phi > 0$ everywhere. With x and y the independent variables, the Euler equations for the mesh can be written

$$0 = -\frac{\partial}{\partial x}(wJ^2), \qquad 0 = -\frac{\partial}{\partial y}(wJ^2). \tag{49}$$

When $x_\eta = y_\xi = 0$, and all derivatives of ϕ in y are zero, it follows that

$$\frac{\partial J}{\partial y} = 0 = \frac{x_\xi J_\eta}{J} = \frac{1}{J}(x_\xi^2 y_{\eta\eta}). \tag{50}$$

That is, the mesh spacing is constant in y. Thus, the mesh spacing in x must vary as in the one-dimensional case,

$$\left(\frac{1}{\phi}\frac{\partial \phi}{\partial x}\right)^2 x_\xi^2 = \frac{c}{y_\eta^2} = C. \tag{51}$$

For other directions of shock propagation, the equations will also reduce because the variational principle is invariant under rotation. In general, J will vary most strongly in the direction $\nabla\phi/\phi$ so that the number of mesh points is increased in the direction of greatest variation of the data.

The following example illustrates the application of the adaptive mesh to a singular perturbation problem. Consider the convection, diffusion equation

$$\phi_t + \nabla \cdot \phi \mathbf{U} - \kappa \nabla \cdot \nabla\phi = 0, \tag{52}$$

where $\mathbf{U} = \hat{r}U(r)$ is given and $\kappa > 0$. On an infinite domain, stationary solutions result when

$$\mathbf{U}\phi - \kappa \nabla\phi = 0. \tag{53}$$

In solving this equation numerically, errors in representing $\nabla\phi/\phi$ usually result in solutions corresponding to $\kappa' > \kappa$. That is, the numerical solutions correspond to a larger diffusivity than the one intended because of numerical error. Thus, the maximum error

$$\varepsilon = \max \left| \mathbf{U} - \frac{\kappa \nabla\phi}{\phi} \right| \tag{54}$$

measures how closely the numerical solution approaches the correct one. In the following discussion, the effect of adapting the mesh on the error ε will be shown.

When $U(r)$ is given by

$$U(r) = -rU_0^2 h^+ h^-/\kappa, \tag{55}$$

where

$$h^\pm = \left[1 + \exp \frac{\pm U_0(r - r_0)}{\kappa}\right]^{-1}, \tag{56}$$

the steady solution to the convection diffusion equation can be written

$$\phi(r) = \phi(0) \exp\left\{\frac{U_0}{\kappa} r h^+ - \frac{\kappa}{U_0} \ln \frac{h^-}{h^+}(r = 0)\right\}. \tag{57}$$

The solution is of the same form as that for Burger's equation but for the corrections for cylindrical geometry, and a similar singularity in ϕ develops in an annulus at $r = r_0$ as $\kappa \to 0$.

The singular behavior of ϕ is treated similarly to Burger's equation in one dimension.

To measure the decrease in ε resulting from adapting the mesh, the following experiment is performed. On a computation mesh with vertices (x_{ij}, y_{ij}) $i = 1, M$; $j = 1, N$, ϕ is evaluated at the center of each cell. Using ϕ, the weight function is calculated from the equation

$$w_{ij} = \left\langle \frac{1}{\phi}\frac{\partial \phi}{\partial x} \right\rangle_{ij}^2 + \left\langle \frac{1}{\phi}\frac{\partial \phi}{\partial y} \right\rangle_{ij}^2, \tag{58}$$

where the difference equations are in the form sometimes used in Lagrangian fluid codes [22, 23],

$$\begin{aligned}\left\langle \frac{1}{\phi}\frac{\partial \phi}{\partial x} \right\rangle_{ij} = [&\phi_{i-1,j}(y_{ij+1} - y_{ij-1}) + \phi_{i-1j-1}(y_{i-1j} - y_{ij-1}) \\ &+ \phi_{ij-1}(y_{ij-1} - y_{i+ij}) + \phi_{ij}(y_{i+1j} - y_{ij+1})]/\bar{\phi},\end{aligned} \tag{59}$$

and

$$\begin{aligned}\left\langle \frac{1}{\phi}\frac{\partial \phi}{\partial y} \right\rangle_{ij} = -[&\phi_{i-1j}(x_{ij+1} - x_{ij-1}) + \phi_{i-1j-1}(x_{i-1j} - x_{ij-1}) \\ &+ \phi_{ij-1}(x_{ij-1} - x_{i+ij}) + \phi_{ij}(x_{i+1j} - x_{ij+1})]/\bar{\phi},\end{aligned} \tag{60}$$

where $\bar{\phi}$ is given by

$$\begin{aligned}\bar{\phi} = \{&\phi_{i-1j}[(x_{ij+1} + x_{ij})(y_{i-1j} - y_{ij}) - (x_{i-1j} - x_{ij})(y_{ij+1} - y_{ij})] \\ &+ \phi_{i-1j-1}[(x_{i-1j} - x_{ij})(y_{ij-1} - y_{ij}) - (x_{ij-1} - x_{ij})(y_{ij-1} - y_{ij})] \\ &+ \phi_{ij-1}[(x_{ij-1} - x_{ij})(y_{i+1j} - y_{ij}) - (x_{i+1j} - x_{ij})(y_{ij-1} - y_{ij})] \\ &+ \phi_{ij}[(x_{i+1j} - x_{ij})(y_{ij+1} - y_{ij}) - (x_{ij+1} - x_{ij})(y_{i+1j} - y_{ij})]\}.\end{aligned} \tag{61}$$

Although it is peripheral to the discussion, it must be noted that it is useful to prepare w for the calculation by smoothing and scaling it as follows. Because the difference equation above "roughens" the data causing the adaptive mesh to respond to spurious changes in w on the scale of one cell width, the smoothing equation

$$w_{ij}^{(l+1)} - w_{ij}^{(l)} = \nu\{(w_{i+ij}^{(l)} + w_{ij+1}^{(l)} + w_{i-ij}^{(l)} + w_{ij-1}^{(l)})/4 - w_{ij}^{(l)}\}, \tag{62}$$

is solved two or three times. To provide external control of the range of variation, w_{ij} is scaled as follows. So that comparable adjustments of the vertex positions produce

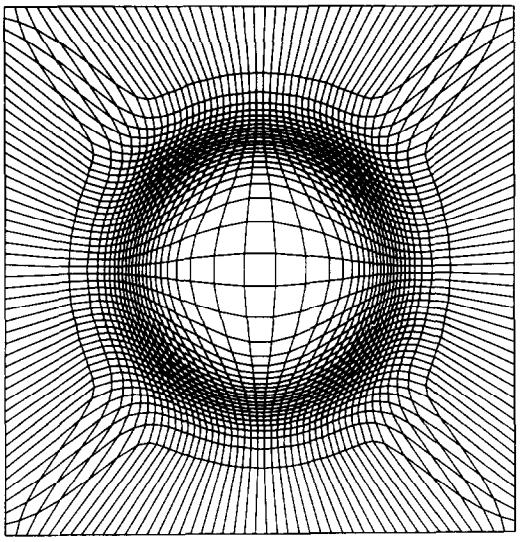

FIGURE 12

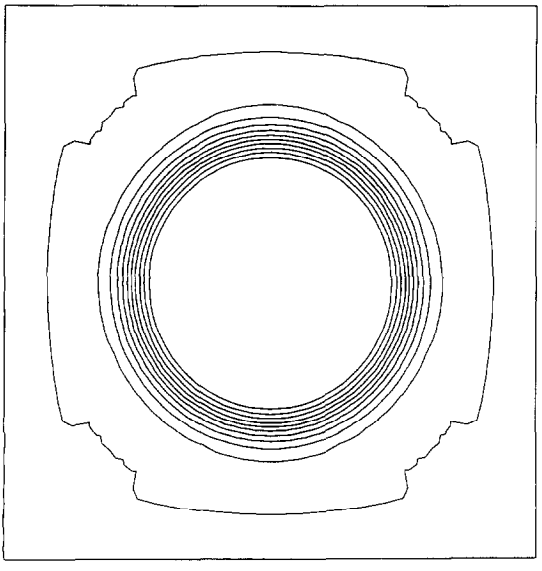

FIGURE 13

FIGS. 12 and 13. Using the volume control, the mesh shown in (12) has been adapted to increase the resolution of a function whose contours, shown in (13), indicate rapid variation in a narrow annulus. The resolution in (12) is increased at the expense of increasing the size of the zones exterior to the annulus.

comparable changes in the value of I_s and I_v, the contribution of each cell to I_v is made equal to one by scaling w' in the limit $\lambda_v \to \infty$ such that

$$w'_{ij} J_{ij}^2 = 1. \tag{63}$$

The range of variation of w' is determined by the lesser of the externally set value σ_0 and the ratio of the weight function

$$\sigma = \min \left[\sigma_0, \frac{\max_{i,j}(w_{ij})}{\min_{ij}(w_{ij})} \right]. \tag{64}$$

So that the largest zone fits in the computational domain, the minimum value of w, q, must satisfy the equation

$$q = \min_{ij} (w'_{ij}) = \min \left[\frac{1}{\sum_{ij} (J_{ij})^2}, \frac{1}{\sigma} \right]. \tag{65}$$

The scaled w' is calculated from

$$w'_{ij} = q \left[\frac{(\sigma^2 - 1)\, w_{ij}}{\max_{ij}(w_{ij})} + 1 \right]. \tag{66}$$

Using w'_{ij}, the combined Euler equations (12), (16), and (19) are solved by moving the vertices. On the new mesh, ϕ_{ij} is recalculated and the entire process above is repeated until the Euler equations are satisfied everywhere.

The results of several numerical calculations on a square domain, $0 \leqslant x \leqslant 1$,

variation of ϕ, the contours indicate where $\partial\phi/\partial r$ is large, and thus where the cells must be small. In Fig. 12 an adapted mesh with Dirichlet boundary conditions is shown ($\lambda_v = 2$ and $\sigma_0 = 100$). The zones in Fig. 12 are clearly smaller where the contours are closely spaced in Fig. 13.

The most important result is shown in Fig. 14 where the variation of I_v, I_s and ε with λ_v is shown.

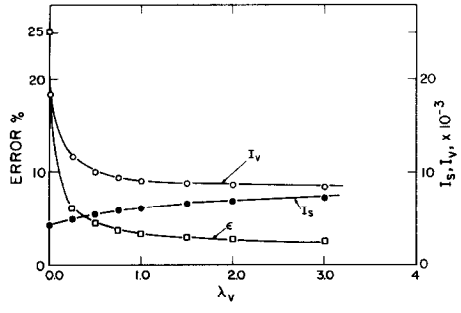

FIG. 14. Minimizing I_v minimizes the numerical error.

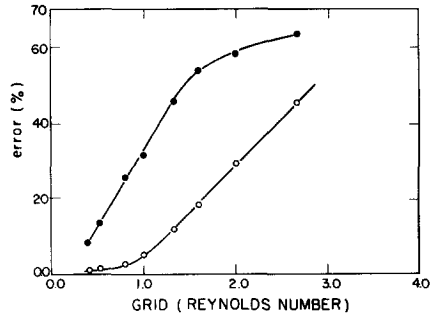

FIG. 15. As the resolution increases, the error for both adaptive (○) and nonadaptive (●) meshes decreases. With the adaptive mesh, however, when the average mesh spacing equals the smallest gradient length ($R_e = 1$), the error is about 5%, one-sixth the value obtained with the nonadaptive mesh.

Clearly, minimizing I_v reduces the error since both I_v and ε decrease together as λ_v increases. The decrease in I_v results in an increase in I_s corresponding to increasing departure from Winslow's mesh: although both I_v and I_s change less rapidly for $\lambda_v > 1$. The decrease in ε as λ_v increases from 0 to 1 is dramatic; from 25 to 3.5%. The subsequent decrease in ε with increasing λ_v is small by comparison. The conclusion is that with $\lambda_v = O(1)$ (much less than the maximum possible value) substantial increases in accuracy are obtained.

The effect of varying M and N is shown in Fig. 15. With $\kappa = 0.025$, $\lambda_v = 3$, $\sigma_0 = 100$, as $M \times N$ increases from 15×15 to 99×99, R_e decreases from 2 to 0.4. The upper curve corresponds to ε for a nonadaptive mesh, the lower to an adaptive mesh. For $R_e < 1$, ε for the adaptive mesh is less than 5%, as little as one-tenth the error in the nonadaptive mesh.

The error scaling with the nonadaptive mesh is shown in Fig. 16, where $\varepsilon R_e/(\sinh(R_e) - R_e)$ is plotted corresponding to $\kappa = 0.05$. The scaling is as predicted

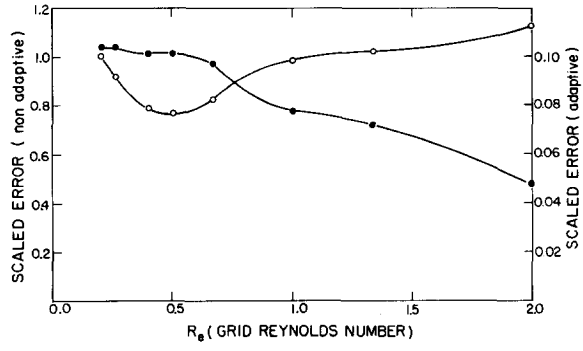

FIG. 16. The scaling of the error for adaptive (○) and nonadaptive (●) meshes is compared with the results of error analysis. For both cases, when $R_e < 1$, the convergence with decreasing R_e is quadratic. Adaptive mesh, ε/R_e^2; nonadaptive mesh, $\varepsilon R_e/(\sinh(R_e) - R_e)$.

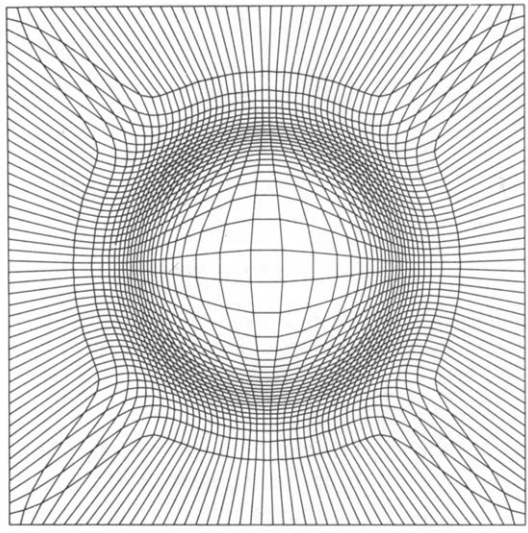

FIGURE 17

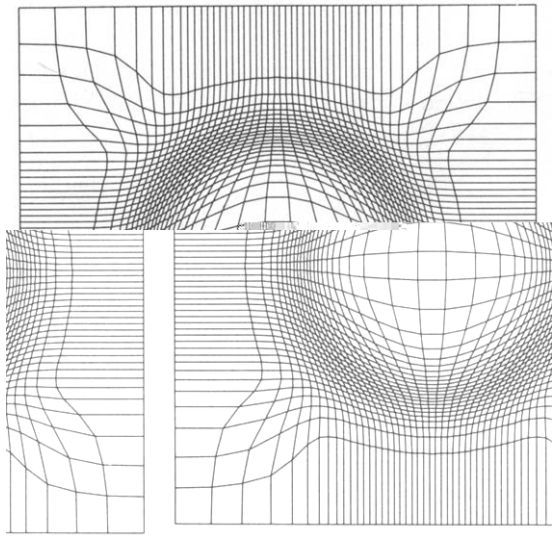

FIGURE 18

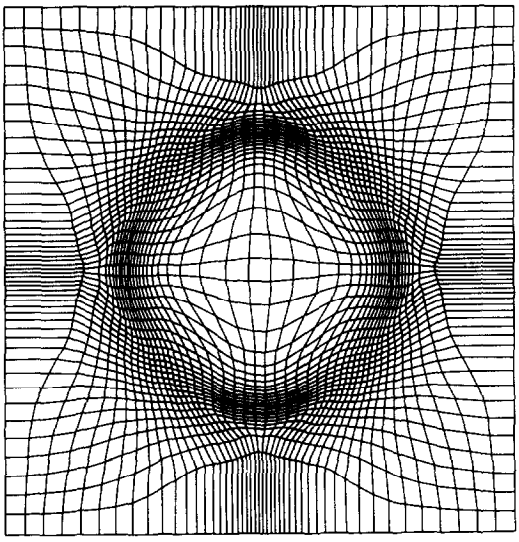

FIGURE 19

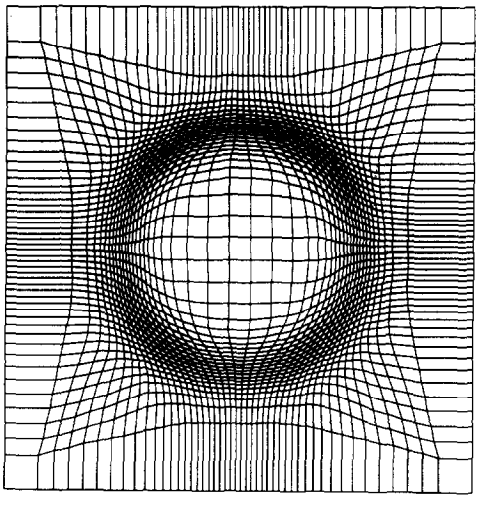

FIGURE 20

FIGS. 17–20. The effect of decreasing skewness on the adaptive mesh shown in Fig. 17 is examined. With orthogonality only at the boundary, Fig. 18 results. Minimizing I_0 (Eq. (3a)) results in Fig. 19, and minimizing I_0' (Eq. (3b)) results in Fig. 20. Only in the case of Fig. 19 does decreasing skewness interfere with adaptivity.

for $R_e < 1$, which essentially means $\varepsilon = O(R_e^2)$ for small R_e. For the adaptive mesh, εN^2 for $\kappa = 0.025$ also is plotted in Fig. 16. The scaling is approximate, but seems to agree with numerical results. The point is, of course, that $R_e^2 = \alpha N^2$ for constant κ, and thus the convergence of ε to zero with $1/N$ for both adaptive and nonadaptive meshes is quadratic for $R_e < 1$. That the scaling is similar suggests that the increased resolution in the singular region reduces the error, but does not give the change in scaling predicted by Eq. (47).

Finally, the effect of simultaneously minimizing I_0 (Eq. (3)) and I_v is examined. In Figs. 17–20, four meshes, all with $M = N = 50$, $\sigma_0 = 100$, $\lambda_v = 2$ and $\kappa = 0.025$, with $\lambda_0 = 0$ and Dirichlet boundary conditions in Fig. 17, with $\lambda_0 = 0$ and orthogonal boundary conditions in Fig. 18, with $\lambda_0 = 1$ and minimizing I_0 (Eq. (3a)) in Fig. 19, and with $\lambda_0 = 1$ and minimizing I_0' (Eq. (3b)) in Fig. 20.

First, we can make some comments on the meshes themselves. Comparing Figs. 17 and 18, the orthogonal boundary conditions appear to reduce the skewness of the cells in the corners of the mesh without affecting the interior. Comparing Figs. 19 and 20 indicates that the volume weighted orthogonality minimization (I_0') affects corner cells and the interior, but not the cells in the singular region. By contrast, the minimization of I_0 significantly reduces the skewness of the small cells in the singular region. Because of this, we may expect minimization of I_0 to compete more than I_0' with the minimization of I_v.

Evidence of the competition is shown in Fig. 21, where I_v and ε are plotted against λ_0 when minimizing I_0 and I_0'. When I_0 is minimized, both ε and I_v increase with λ_0. In the case of ε, the increase is nearly 100%. When I_0' is minimized, I_v increases somewhat, but the increase in ε is small ($\sim$5%). Evidently, minimizing I_0' is more compatible with the adaptive algorithm than minimizing I_0.

We must note, however, that minimizing I_0 or I_0' and I_v simultaneously does not yield an orthogonal mesh. Effective volume control (with the contraint that connectively be preserved) seems to introduce some skewness. Eliminating the skewness results in less effective volume control. On the other hand, reducing skewness by orthogonal boundary conditions as shown in Figs. 17 and 18 actually increases the error by our measure from 7.5% (denoted by an x in Fig. 21) to 9.6%.

VII. Conclusion

This description of work on adaptive meshes is necessarily incomplete. Among the areas not covered, but where there are results, are the application of the adaptive mesh to time-dependent problems [16, 17], and its extension to three dimensions and to non-Cartesian coordinates.

There are also many unanswered mathematical questions. For example, is the difficulty in obtaining solutions for large λ_0 and λ_v mathematical or numerical in origin? For more complicated systems of equations, how can the choice of weight functions to minimize error be tested a priori?

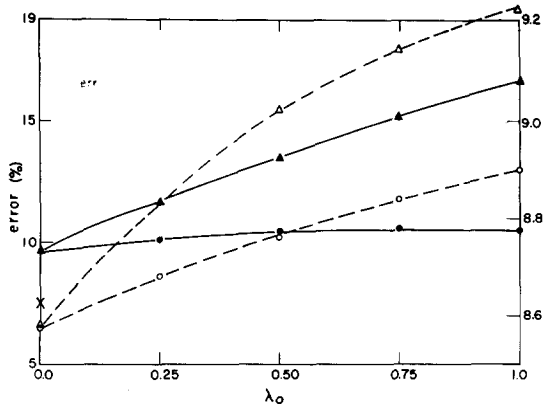

FIG. 21. When I_0' is minimized, the value of I_v does not change indicating compatibility. When I_0 is minimized, however, I_v increases. Thus Thus, I_0' is suitable for decreasing the skewness of adaptive meshes, but I_0 is not. Minimize I_0: ▲, error; △, I_v. Minimize I_0': ●, error; ○, I_v.

In spite of all the areas not discussed, a systematic method for measuring desirable mesh properties using several integral measures has been presented. By forming a variational principle using linear combinations of the integral measures, a system of partial differential equations was derived. These equations were solved numerically using a relaxation algorithm. The effect of each term in the variational principle on the mesh has been demonstrated. The ability of the mesh technique to resolve singular problems in one and two dimensions was also shown.

ACKNOWLEDGMENTS

Helpful discussions with E. Isaacson, P. Lax, and C. Peskin are gratefully acknowledged. This work was supported by the U. S. Department of Energy.

REFERENCES

1. A. M. WINSLOW, *J. Comput. Phys.* 1 (1966), 149.
2. S. K. GODUNOV AND G. P. PROKOPOV, *USSR Comput. Math. Phys.* 12 (1972), 182.
3. J. F. THOMPSON, F. C. THAMES, AND C. W. MASTEN, *J. Comput. Phys.* 15 (1974), 299.
4. J. L. STEGER AND R. L. SORENSEN, *J. Comput. Phys.*, to appear.
5. H. A. DWYER, R. J. KEE, AND B R. SANDERS, "An Adaptive Grid Method for Problems in Fluid Dynamics and Heat Transfer," AIAA 79-1464.
6. R. G. HINDMAN, P. KUTLER, AND D. ANDERSON, "A Two-dimensional Unsteady Euler-Equation Solver for Flow Regions with Arbitrary Boundaries," AIAA 79-1465.
7. T. H. CHONG, *SIAM J. Numer. Anal.* 1 (1978), 2.
8. W. GROPP, *SIAM J. Sci. Statist. Comput.* 1 (1980), 2.
9. R. J. GELINAS, S. K. DOSS, AND K. MILLER, *J. Comput. Phys.*, submitted.
10. I. BABUSKA AND W. RHEINBOLDT, *SIAM J. Numer. Anal.* 15 (1978), 736.

11. D. C. BARNES *et al.*, *Nucl. Fusion* **21** (1981), 537.
12. J. U. BRACKBILL, *Methods. Comput. Phys.* **16** (1976), 1.
13. P. BROWNE, private communication, Los Alamos Nat. Lab., Los Alamos, N.M.
14. W. D. BARFIELD, *J. Comput. Phys.* **6**(1970), 417.
15. R. COURANT, *Trans. Amer. Math. Soc.* **50** (1941), 40.
16. J. SALTZMAN AND J. BRACKBILL, *Bull. Amer. Phys. Soc.* **25** (1980), 973.
17. R. D. MILROY AND J. U. BRACKBILL, *Bull. Amer. Phys. Soc.* **25** (1980), 833; *Phys. Fluids*, in press.
18. M. M. RAI AND D. A. ANDERSON, "Numerical Grid Generation Techniques," NASA Conf. Publ. 2166, p. 409, 1980.
19. N. N. YANENKO, V. M. KOVENYA, V. D. LISEJKIN, V. M. FOMIN, AND E. V. VOROZHTSOV, "Proceedings, 6th Intern. Conf. on Numerical Methods in Fluid Dynamics," *Lecture Notes Phys.* **90** (1979), 565.
20. J. U. BRACKBILL, *Bull. Amer. Phys. Soc.* **24** (1979), 1095; J. U. Brackbill and J. Saltzman, "Numerical Grid Generation Techniques," NASA Conf. Publ. 2166, 193, 1980.
21. P. P. BELINSKII, S. K. GODUNOV, YU. B. IVANOV, AND I. K. YANENKO, *USSR Comput. Math. Math. Phys.* **15** (1975), 133.
22. C. W. HIRT, A. A. AMSDEN, AND J. L. COOK, *J. Comput. Phys.* **14** (1974), 227.
23. W. F. NOH, *Methods Comput. Phys.* **3** (1964), 117.